2024 IEEE International Conference on Robotics and Automation (ICRA 2024)
May 13-17, 2024. Yokohama, Japan

RETOM: Leveraging Maneuverability for Reactive Tool Manipulation using Wrench-Fields

Felix Eberle[1], Riddhiman Laha[1], Haowen Yao[1], Abdeldjallil Naceri[1],
Luis F.C. Figueredo[2], and Sami Haddadin[1]

***Abstract*— This paper investigates the problem of effective tool manipulation for motion planning in complex human-like scenarios. Vector-field-based real-time strategies, although widely used, usually do not account for unwieldy tools or incorporate systematic methods to handle these extra maneuvers needed. Instead, we formalize the problem and propose a novel field-based reactive planner that explicitly accounts for rotational forces for seamless maneuvers based on the tool's geometry and featured points. Furthermore, we capture and encode robot performance through capability metrics and improve the same using an additional quality distribution method. This enables seamless integration of the robot's embodiment with the reactive force-torque (wrench) field giving rise to flexible tool usage in non-stationary environments. Extensive simulation analysis on a 7 DoF collaborative robot manipulating a common tool in an unorganized table-top layout reinforces our claim of robustness in stationary and non-stationary scenarios.**

I. Introduction

Constructive tool usage in complex tasks is considered by many to be a hallmark of general intelligence [1], [2]. In the robotics context, when manipulating objects and tools in cluttered environments, additional issues like rotational maneuvers need to be taken care of, as they reduce the robot's free configuration space and cast supplementary constraints in workspace [3]. Therefore, for intelligent decision-making, these skills need to be grounded in an embodied structure capturing the robot's performance. Similar to human manipulation [4], robots need to have intrinsic knowledge of their feasible postures to meet the arising manipulation challenges.

As an example, consider the case of manipulating an elongated tool (like a hammer) in an unstructured environment as depicted in Fig. 1. Intuitive to what we humans do, a robot should make use of local reactive maneuvers while also planning moving towards in the goal in configurations with sufficient ability to perform these maneuvers. Ideally, the model for scenarios like this should encode a rotational component that re-orientates the tool in a reactive fashion in the 6D space—which in turn is only feasible in high maneuverability workspace.

Most of the scarce works on tool manipulation in collision-free space emphasize offline solutions. For example, Stillman and Kuffner [5] deploy a modified RRT-Connect algorithm for sampling future paths with handheld tools [6]. Similar roadmap-based strategies for object retrieval in cluttered areas are presented in [7], [8]. Additional research has been conducted on tool usage in a task and motion planning [9] and sequential planning [10]–[12]. However, the offline nature limits their application in semi-structured contexts. In fast-changing situations, constraint manifolds sampling requires sophisticated strategies that might not capture object-environment affordances [13], [14]. Moreover, interactions between the held tool and dynamic obstacles are rarely considered by the high dimensional manipulation planners in the literature. Recently, there has been a push toward generating motion policies that exploit the geometric structure of the task space for principled vector-field constructions [15]–[17]. Our long-term goal is to utilize these concepts for computing motion plans for general tool usage in complex and non-stationary scenarios.

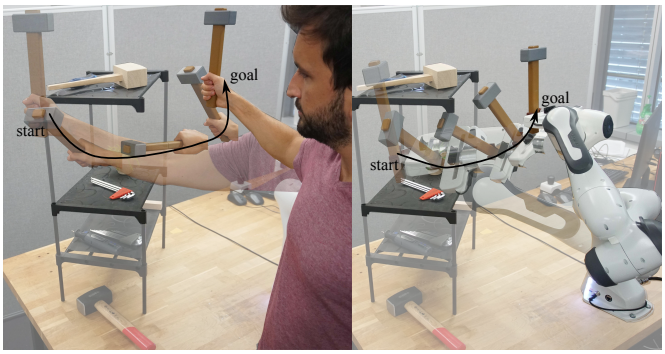

Fig. 1. Tool manipulation for planning in constrained environments. *Left*. Humans intuitively combine wrist rotation and translation movements to avoid collision while keeping good manipulability along the path (black solid line). *Right.* We instill a similar capability for a robot motion planning task based on reactive forces for collision avoidance and torques along the tool geometry for tool rotation while actively seeking high maneuverability.

A more promising paradigm is the use of reactive task-space motion generation strategies (see, e.g., [18]–[25]) which often produce trajectories suitable for real-time obstacle avoidance and compensation, thanks to their close alignment with the actuation space [26]. Specifically, vector-field-based approaches [27]–[29] enable smooth reactive maneuvers, bridging the gap between planning and robot control. The seminal work [18] used the electro-static potential concepts, while circular fields (CF)-based planning [21], [30] emerged as a notable variant. Our prior research shows that CFs can effectively manage reactive strategies around both stationary and dynamic objects in both individual [24] and constrained dual-arm scenarios [31], [32].

Although these methods are effective for 3D Cartesian

[1]The authors are with Munich Institute of Robotics & Machine Intelligence, Technische Universität München (TUM), Germany.

[2]L. Figueredo is with the School of Computer Science, University of Nottingham, UK. L. Figueredo is also an Associated Fellow at the MIRMI, Technical University of Munich (TUM). Email: figueredo@ieee.org

This work was funded by the Lighthouse Initiative Geriatronics by StMWi Bayern (Project X, grant 5140951), LongLeif GaPa gGmbH (Project Y, grant 5140953). Email:{felix.eberle, riddhiman.laha, haowen.yao, djallil.naceri, haddadin}@tum.de

evasion strategies, they fail to capture tool flexibility in cluttered scenarios. Furthermore, more posture adaptability is needed for systematic integration of tool geometry. Therefore, in this work we present a reactive tool handling strategy that builds on our previous work [26], adding a locally reactive rotational component activated by the tool's proximity and orientation towards obstacles. This results in a six dimensional force-moment pair (wrench) that extends the translational avoidance of previously mentioned vector-field-based approaches, creating a *wrench-field*. A key enabler in this regard is our integration of the maneuverability maps, which leverage robot capability information [33]–[37], in order to direct the system to regions of higher performance.

Separately, both reactive planning and quality-index maps are established areas within robotics research. However, to the best of the authors' knowledge, no results have leveraged easy-to-obtain reliable information of the robot's workspace – in our case, maneuverability – with locally reactive planners. Merging maneuverability maps with real-time responses from wrench-fields reinvigorates the reactive planning framework and allows for informed reactiveness and flexibility required for manipulating tools and objects. We name this approach REactive TOol Maneuvers (RETOM).

Contributions: Our contributions to the state-of-the-art are the following: (i) A real-time modular framework that extends current state-of-the-art vector-field-based algorithms through wrench-fields (ii) Introduction of reactive rotational evasions of end-effector-tool system depending on its configurations in relation to obstacles; (iii) Integration of maneuverability maps to encapsulate global feasibility and manipulability information to intelligently guide maneuvers towards improved workspace regions.

II. Overview and Problem Statement

We formalize a performance-induced manipulation planning algorithm as a dynamical system. Our main intention is to enhance existing vector-field-based methods with robot capability information such that feasible trajectories are generated utilizing global knowledge.

A. Terminology

1) Wrench-Fields: For computation of reference control signals, we generate navigation wrenches $\boldsymbol{\mathcal{F}}_{\text{nav}} \in \mathbb{R}^6$ in the workspace. When the tool polyhedron (see Fig. 3) is outside the proximity sphere of the obstacles, the moment component becomes inactive. On the other hand, when the polyhedron interpenetrates the sphere, we obtain an active force and moment pair which steers the system through the environment.

2) Maneuverability: We define the capability of the system at a particular local configuration using a normalized metric w. We call this our *maneuverability metric*. This is computed and encoded using our defined data structure $\mathcal{V}$ containing information for each voxel $\boldsymbol{v}$ of the voxelized task-space.

B. Problem Formulation

Let $\mathcal{S} \in SE(3)$ be the task-space of the robot and $\mathcal{S}_{\text{obs}} \subset \mathcal{S}$ be an infeasible set of task-space regions occupied by obstacles. The free region is denoted by $\mathcal{S}_{\text{free}} = \mathcal{S} \setminus \mathcal{S}_{\text{obs}}$. Let $\boldsymbol{s}_{\text{start}} \in \mathcal{S}_{\text{free}}$ be the initial starting point of the planning process and $\boldsymbol{s}_{\text{goal}} \in \mathcal{S}_{\text{free}}$ be the final desired goal state. We define $\boldsymbol{v}_{\text{attr}}$ as the set of transitional attractors in $\mathcal{S}_{\text{free}}$.

Problem Statement 1. *Given $\boldsymbol{s}_{\text{start}}$ and $\boldsymbol{s}_{\text{goal}}$, find a feasible path $\mathbb{P}$, passing through the elements of $\boldsymbol{v}_{\text{attr}}$, in $\mathcal{S}_{\text{free}}$ such that w is maximized (robot passes through regions of larger maneuverability).*

In other words, the goal of the proposed planning scheme is to design a reactive evasive maneuver based on our wrench-field that guides the robot's end-effector-tool system. For the purpose of the study, we make the following assumptions: (i) the end-effector-tool system is rigidly connected (firm grasp), (ii) the tool admits an allowable deflection in the form of 'wrist' rotation, and (iii) that the robot's kinematic structure is known beforehand. Presently, we are interested in evasive maneuvers for the robot end-effector, but our algorithm is general enough to be extended to whole body collision avoidance [38].

Our problem follows and extends the reactive motion generation paradigm [24]–[27], [30], [31], which defines $\boldsymbol{s}_{\text{goal}}$ as a basin of attraction to a force vector-field $\mathbf{F}_{\text{a}}$. This field interacts with a guiding CF force $\mathbf{F}_{\text{c}}$ stemming from multiple static and dynamic obstacles to produce a resulting force vector-field that guides the robot-tool system towards the $\boldsymbol{s}_{\text{goal}}$ in the unobstructed space $\mathcal{S}_{\text{free}}$. However, many such strategies don't account for the robot's kinematic structure and constraints. Even if the force field leads the robot to a feasible task-space position within $\mathcal{S}_{\text{free}}$, it might be infeasible in the joint space due to joint limits and singularities.

Our approach differs by taking into account the robot's kinematics. Maneuverability, as illustrated in Fig. 2, combines the robot's manipulability from [39] and the number of feasible nullspace solutions (maximum of 24 is possible).

Feasible orientations for the end-effector are also considered by our planner apart from maneuverability information and obstacle locations. Further, it examines the allowable deflection of the tool, enabling movement through narrow passages. This adds additional freedom to the reactive planning strategy.

III. RETOM Algorithm

In this section, we first illustrate the wrench-field-based motion generation and obstacle evasion framework. Next, we explain how maneuverability maps are used for attractor placement to reach the final goal. Finally, we introduce the reactive tool rotation (RTR) algorithm, which ensures local flexibility of the manipulated object for task success.

A. Motion Generation and Obstacle Avoidance Strategy

The robot end-effector is guided through the workspace by a steering wrench $\boldsymbol{\mathcal{F}}_{\text{nav}}$. It consists of an attractive potential force $\mathbf{F}_{\text{a}} \in \mathbb{R}^3$ causing a translation towards the goal $\boldsymbol{s}_{\text{goal}}$, as well as a locally reactive circular field force $\mathbf{F}_{\text{c}} \in \mathbb{R}^3$ and the reactive tool torques $\boldsymbol{\tau}_{\text{rot}} \in \mathbb{R}^3$ enabling obstacle avoidance:

$$\boldsymbol{\mathcal{F}}_{\text{nav}} = \begin{bmatrix} \mathbf{0} \\ \mathbf{F}_{\text{a}} \end{bmatrix} + \begin{bmatrix} \mathbf{0} \\ \mathbf{F}_{\text{c}} \end{bmatrix} + \begin{bmatrix} \boldsymbol{\tau}_{\text{rot}} \\ \mathbf{0} \end{bmatrix} . \tag{1}$$

The virtual potential field causing the attractive force, towards the desired goal $\boldsymbol{x_d}$ is a proportional signal as described in [31]. While this approach has been applied with repulsive forces for obstacle avoidance [18], they are prone to getting

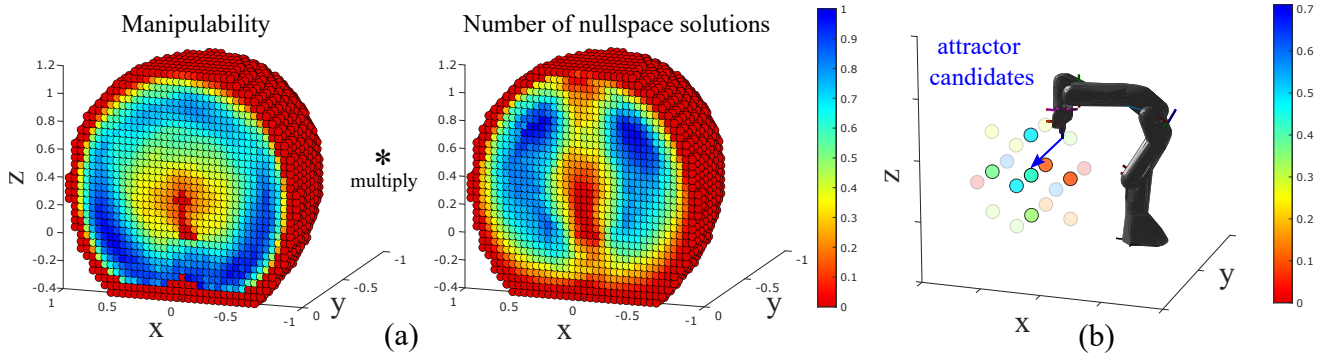

Fig. 2. Maneuverability information of the voxelized workspace of the Franka Emika research robot. (a) We combine the map constructed using the manipulability metric with the map encoding the number of nullspace solutions to generate the maneuverability map shown in (b). This new map is then exploited to strategically select regions for intermediate (feasible) target placement for the wrench-field that results in better kinematic flexibility.

stuck in local minima for certain obstacle arrangements and geometries [40]. Thus, circular fields are employed for local-minima free[1] obstacle avoidance of the robot end-effector. Additionally, we introduce reactive tool rotation for extending obstacle avoidance to the object held by the robot. Both strategies are elaborated upon in subsection III-C.

One issue with combining global goal attraction and local obstacle avoidance is that it can often result in convoluted paths. This happens because obstacle information is only used for motion generation when the robot is near the obstacle, leading to locally reactive force application. As a result, the robot might backtrack or maneuver into trap-like situations. As experimentally shown in the ablation studies in IV-C, avoidance using circular fields can push the robot into areas with poor manipulability or even infeasible orientations, which directly affects tool handling capabilities. To address these challenges, a planner that uses both obstacle and manipulability information is proposed.

B. Global Planning Perspective using Maneuverability Maps

In this section, we describe how maneuverability information is used as an additional metric to guide the planner toward obstacle-free areas of greater manipulability, enhanced rotation options, and increased possible nullspace motion. Like human manipulation, robots should explore posture configurations that optimize the task by exploiting their kinematic structure.

1) Precomputed Voxelized Map: To generate the maneuverability map, we discretize the $SE(3)$ workspace, the space of all end-effector (EE) positions and orientations. To this end, the Cartesian 3D space is uniformly discretized with a resolution of $0.1\,\mathrm{m}$ into N_{pos} positions. For each N_{pos}, we discretize N_{dir} z-axis directions and N_{rot} rotations around one z-axis direction of the EE. If it is a feasible configuration for the robot, the data is then organized as a rigid body transformation $\mathcal{T}_{\mathrm{EE}} = \{\boldsymbol{T}_{\mathrm{EE}(pos,dir,rot)}\}$.

A scoring function is then used to assign a quality index, termed *maneuverability*. This maneuverability is scored according to the following: (a) the manipulability measure m (b) the number of possible n-nullspace solutions within the discretized swivel angle space [37]. [2]

[1]See the results in [21] for the specific conditions.

[2]Herein, a maximum of 24 different nullspace configurations for each of the same 6D voxel are evenly explored ($N_{\mathrm{dir}} = 5$ and $N_{\mathrm{rot}} = 20$).

The manipulability measure m for each configuration is defined as proposed in [39],

$$m = \sqrt{det(JJ^T)} = s_1 s_2 \dots s_n, \tag{2}$$

where J is the geometric Jacobian of the manipulator and s_i denotes the singular values such that the measure ensures proportionality to the manipulabilty ellipsoid volume. In other words, the smaller the value of s_i is, the closer is the current configuration to a singular pose. To calculate our maneuverability score for a specific position, we take the median of the manipulability of all viable configurations over each position and normalize it (since m is not a bounded performance index [41]) to $\hat{m}$ with reference to the highest achievable value in the entire robot's workspace. The number of possible nullspace solutions n also takes the median of each orientation and is normalized to $\hat{n}$ to be used as an additional scoring factor to favor position with many viable configurations. We can then calculate our maneuverability score with a value between 0 and 1 according to

$$w = \hat{m} \cdot \hat{n}. \tag{3}$$

Each discretized position corresponds to a 3D voxel $\boldsymbol{v}$ in the resulting map (see Fig. 2).

2) Maneuverability-informed Intermediate Target Assignment: To leverage the robot's advantageous posture(s) during motion execution, we utilize the maneuverability map generated in the previous subsection. To this end, we introduce the maneuverability-informed Intermediate Target Assignment (MITA) algorithm. The aim is for MITA to target high scoring regions in the workspace $\mathcal{V}_{\text{scored}}$, which is the set of all scored voxels. Throughout the motion execution, the algorithm continuously monitors the obstacle location and the predicted path to the goal in an online fashion with a frequency of 10Hz. It determines if an obstacle (approximated by spheres) intersects with a voxel and penalizes it based on a distance related metric. The proposed methodology involves assessing neighboring voxels in proximity to the predicted path where the maneuverability and also traversability of the robot is higher and deploy temporary attractors to enable movement through regions in the workspace.

As illustrated in Algorithm 1, the predicted path, represented by the ordered set of traversed voxels $\mathcal{V}_{\text{path}}$, is continuously monitored for traversed voxels $\boldsymbol{v}_i$ that have been assigned a score below our predefined acceptable

Algorithm 1: Intermediate Target Assignment

```
function MITA(v_current, v_goal, V_scored)
    v_attr ← v_goal;
    calculate V_path(v_current, v_goal, V_scored);
    if w_i(v_i) ∈ V_path < w_min then
        w_min,new ← w_i(v_i);
        v_j ← Get new voxel (V_cand, d_main);
        for v_j in V_cand do
            calculate V_path,j(v_current, v_j, V_scored);
            if all w_j in V_path,j > w_min,new then
                v_attr ← v_j;
                w_min,new ← min[w] along V_path,j;
            else if w_min,new = 0 then
                v_attr ← v_start;
            end
        end
    end
    return v_attr;
end
```

threshold w_{min}. This threshold was established on preliminary simulations. If a voxel with a score w is identified such that

$$w_i(\boldsymbol{v}_i) = \min([w_1(\boldsymbol{v}_{\text{start}}), \dots, w_n(\boldsymbol{v}_{\text{goal}})]) < w_{\text{min}}, \quad (4)$$

the eight neighbouring voxels of $\boldsymbol{v}_i$, lying in the plane perpendicular dominant passing direction $\boldsymbol{d}_{\text{main}}$ are considered the set of voxels $\mathcal{V}_{\text{cand,x}}$. Here, x denotes the dominant direction and the voxel candidates would lie in the y-z-plane. We then evaluate these voxels. This results in selecting one with a superior score, which is chosen as an intermediate attractive point, provided the new path traverses only voxels with scores exceeding the one we want to avoid. This process is repeated as the robot advances along the new path until either the goal is reachable again or a voxel along the path now falls below our threshold, for example because the path becomes obstructed by a dynamic obstacle. Our heuristic for terminating MITA is that all the neighboring nodes (entire 3×3-grid) of the blocked voxel are rendered infeasible. This breaks the loop and a workspace check is required.

C. Locally Reactive Tool Handling

Dynamic obstacle avoidance cannot be fully ensured by the placement of intermediate attractive goals alone and must be supplemented with circular fields for locally reactive motion generation. Furthermore, depending on the geometry of the object held by the robot, translation of the end effector may not be sufficient to avoid a collision. Both concepts are described in more detail below.

1) Circular Fields: Unlike the electro-static principles the artificial potential fields are based on, circular fields are derived from the magnetic fields caused by electro-dynamic current flows, which apply a force to a charged particle moving through its field. For our framework we implemented the adaptation by Laha et al. [26] of the aforementioned approach to spherical obstacle geometries. By utilizing a vector $\boldsymbol{l}$ perpendicular to the line connecting the robot end effector with the goal and ensuring that the magnetic field $\boldsymbol{B}$ is perpendicular to both it as well as the robot velocity, it is ensured that the robot is pushed away from the obstacle.

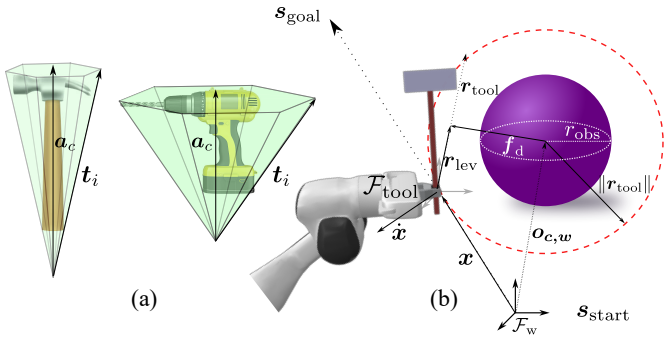

Fig. 3. (a) Common convex work tools such as hammer and a drill modelled as 3D polyhedrons for our calculation of $\boldsymbol{r}_{\text{tool}}$. (b) Reactive tool polyhedron rotation. The red dotted line represents the sphere of the influence of the purple obstacle. $\boldsymbol{r}_{\text{tool}}$ represents the tool axis that is computed from the tool polyhedron $\mathcal{P}_t$. $\boldsymbol{x}$ represents the current heading direction of the robot end-effector. $\boldsymbol{r}_{\text{lev}}$ along with $\boldsymbol{f}_{\text{d}}$ generates the torque $\boldsymbol{\tau_{rot}}$ and creates the reactive tool rotation.

This yields the calculation of the circular force

$$\mathbf{F}_{\text{c}} = \frac{k_c}{d^2 + d_0} \left(\dot{\boldsymbol{x}} \times (\dot{\boldsymbol{x}} \times \frac{\boldsymbol{l}}{\|\boldsymbol{l}\|}) \right). \quad (5)$$

where k_c and d_0 are constants and d is the shortest distance between the robot end effector and the obstacle surface.

2) Reactive Tool Polyhedron Rotation: For handling unwieldy tools in cluttered environments, there might not be a viable path to the goal if there is no systematic change of rotation in translatory movement induced by forces acting directly on the EE. To utilize obstacle information for reactive evasive maneuvers, as demonstrated in Algorithm 2, while maintaining the favorable characteristic from circular fields of goal convergence, we propose applying a virtual torque to the robot-held tool. This facilitates obstacle avoidance through rotation of the EE, with the translatory velocity remaining unaffected.

We consider the manipulation polyhedron $\mathcal{P}_t$ to be the convex hull of the (finite) set of the tool vertices. Let $\boldsymbol{t}_i$ be the vectors along the polyhedron's leading edge, and $\boldsymbol{a}_c$ its central axis (see Fig. 3a). The vector $\boldsymbol{r}_{\text{tool}}$ used for our computation is the vertex $\boldsymbol{t}$ closest to the shortest line connecting the obstacle center to the central axis $\boldsymbol{a}_c$.

The underlying idea of the approach is to have a virtual charged particle on the tool axis $\boldsymbol{r}_{\text{tool}}$ fixed in the EE frame $\mathcal{F}_{\text{tool}}$, with a similar charge as the obstacle. If specific geometric and kinematic conditions between the robot and obstacle are satisfied, a virtual repulsive force enacts a moment and thus a rotation in the fulcrum, the robot EE in our case. For clarity, we introduce the different vectors (see Fig. 3b) considering one obstacle with a radius of r_{obs}. The center of this obstacle, when expressed in the tool frame $\mathcal{F}_{\text{tool}}$ is given by $\boldsymbol{o_{c,tool}}$. The resulting virtual force vector aligns with the shortest distance between the obstacle center and the tool axis. We denote this by $\boldsymbol{f}_{\text{d}}$ and is computed via

$$\boldsymbol{f}_{\text{d}} = \underbrace{\boldsymbol{r}_{\text{tool}} \frac{\langle \boldsymbol{o_{c,tool}}, \boldsymbol{r}_{\text{tool}} \rangle}{\|\boldsymbol{r}_{\text{tool}}\|}}_{\text{lever}} - \boldsymbol{o_{c,tool}}. \quad (6)$$

Note that the bracketed quantity represents the lever arm for our moment and is represented by $\boldsymbol{r}_{\text{lev}}$. Thus, the moment

Algorithm 2: Reactive Tool Rotation (RTR)

```
function RTR(o_c, r_obs, P_t)
    r_tool ← Get tool reaction axis (P_t);
    f_d ← Get force vector (r_tool, o_c);
    while Condition (I) && Condition (II) && Condition (III) do
        for all obstacles do
            τ_rot_i ← Get reactive tool torques (f_d);
        end
    end
    return Total reactive torques τ_rot;
end
```

Algorithm 3: Full procedure for finding final path

```
procedure RETOM()
    while goal not reached do
        v_attr ← MITA(v_current, v_goal, V_scored);
        F_a ← compute attractive force(v_attr);
        F_c ← compute circular force(v_goal, O);
        F_nav ← RTR(r_tool, o_c, r_obs, P_t);
        Δx ← displacement F_nav;
        Δq ← CLIK planning Δx;
        update robot joints Δq;
    end
end
```

generated in the EE can be described as,

$$\boldsymbol{\tau}_{\text{rot}} = k_t \left(\boldsymbol{r}_{\text{lev}} \times \frac{\boldsymbol{f}_{\text{d}}}{\|\boldsymbol{f}_{\text{d}}\|} \right) \left(1 - \frac{\|\boldsymbol{f}_{\text{d}}\|}{\|\boldsymbol{r}_{\text{tool}}\|} \right), \tag{7}$$

with the positive scalar parameter k_t which acts as a gain. The cross product in the first bracket term provides the rotational vector of the torque, its magnitude depending on the lever length $\boldsymbol{r}_{\text{lev}}$. The second term increases the torque, the shorter the distance between obstacle and tool, facilitating faster evasive rotation.

We now detail the three conditions which determine the activation of the reactive tool torque:

- (I): $\|\boldsymbol{f}_{\text{d}}\| \leq \|\boldsymbol{r}_{\text{tool}}\|$,

To ensure the generated torque in eq. 7 does not change direction, the term $\left(1 - \frac{\|\boldsymbol{f}_{\text{r}}\|}{\|\boldsymbol{r}_{\text{tool}}\|}\right)$ must always be ≥ 0. Thus, the derivation of case (I) is straightforward.

- (II): $\langle \boldsymbol{r}_{\text{lev}}, \boldsymbol{r}_{\text{tool}} \rangle > 0 \wedge \|\boldsymbol{r}_{\text{lev}}\| < (\|\boldsymbol{r}_{\text{tool}}\| + r_{obs})$,

As further illustrated in Fig. 3b, condition (II) ensures that the torque only activates if the repulsive obstacle force is applied in an interval with a safety margin r_{obs} on the tool axis $\boldsymbol{r}_{\text{tool}}$ due to an imminent collision.

- (III): $\langle \dot{\boldsymbol{x}}, (\boldsymbol{o}_{\boldsymbol{c},\boldsymbol{w}} - (\boldsymbol{x} + \boldsymbol{r}_{\text{tool}})) \rangle > 0$.

Condition (III) requires that torque only activates when the robot is moving towards the obstacle and not away from it.

Once at least one of the three conditions is no longer active, the tool is rotated back to its initial orientation by a spring-like behavior after a short delay.

D. Manipulation Planning using RETOM

We compute the final path to the goal building on the previous steps as shown in algorithm 3. More specifically, until we reach the goal MITA generates temporary attraction points in the workspace, after which we compute the attractive and repulsive forces based on the environment modelling. Finally, the RTR algorithm returns the navigation wrench which is then used to compute the task-space displacement. A closed loop inverse kinematics (CLIK) scheme with a geometric Jacobian is used to design a feedback law for the robot control.

IV. Simulation Studies

We demonstrate the efficacy of our algorithms through extended simulation studies on a 7 DOF Franka Emika research robot in CoppeliaSim [42] using the MATLAB version of the DQ Robotics library [43]. To ensure consistency across experiments, we use the same parameters for all reported results. The gains k_a, k_c and k_t are 5.0, 0.5 and 4.0, respectively. The scenarios we consider for the simulations are (a) the robot moving with a manipulation tool polyhedron across a cluttered environment, (b) manipulation planning of a hammer-like tool in a dynamic environment, and (c) ablation studies for individual assessment of contributions. Finally, we also assess the limitations of our approach.

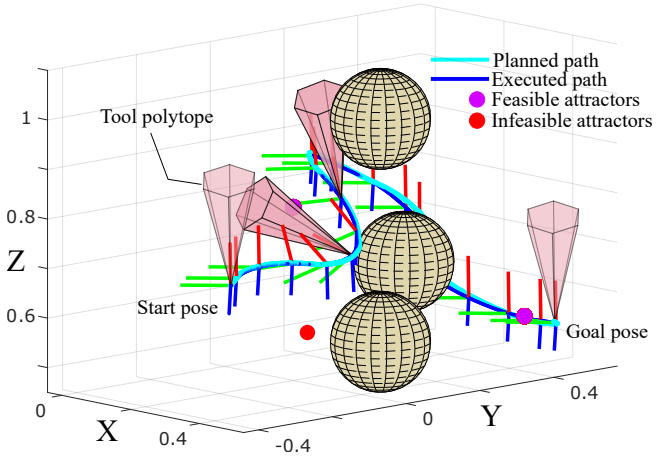

Fig. 4. The robot manipulating a hammer (modeled as the tool polyhedron $\mathcal{P}_t$) in a stationary environment. The reactive tool torques successfully tilt the polyhedron in regions of high maneuverability determined by the intermediate feasible attractors in purple dots.

A. Manipulation of Tools in Clutter

In this experiment, we aim to plan a path within a cluttered 3D environment containing three obstacles. The locations of these obstacles are $[0.4, 0.05, 0.55]$, $[0.4, 0.05, 1.0]$, and $[0.2, 0.30, 0.65]$, each with a radius of 0.1m. Initial starting Cartesian position is $[0.3587, -0.3175, 0.7064]$ and the desired goal is at $[0.4, 0.44, 0.55]$. Fig. 4 illustrates that RETOM successfully plans a collision-free path in this cluttered scene, utilizing intermediate feasible attractor points (denoted in purple). Furthermore, the tilt of the EE frames, due to the reactive tool torques, is evident in trajectory's initial segment.

B. Navigation through Dynamic Obstacles

To assess the robustness of our framework in dynamic environments, we simulated an obstacle crossing the robot's path. Fig. 5 depicts several chronological snapshots of an obstacle passing through the robot's path in a downward

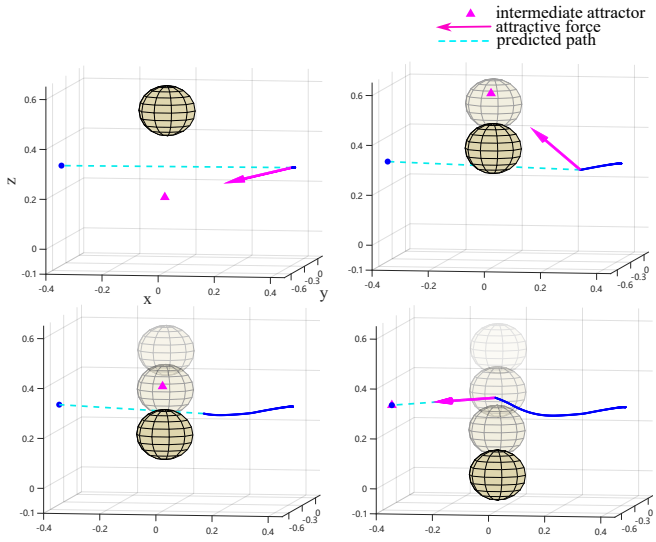

Fig. 5. The dynamic obstacle avoidance path of the robot's end-effector towards the goal (blue). As the obstacle approaches the the predicted path (cyan) intermediate attractive points (pink) redirect the robot until the path toward the goal is viable again. No attractive force is active during the bottom left panel, so as not to counteract the locally reactive CF force.

direction with a velocity of $0.02\frac{m}{s}$. When the obstacle approaches the predicted path towards the goal, the voxels around it are penalized in their score w_i, causing the robot to place intermediate attractors in their vicinity utilizing the MITA algorithm. As soon as the predicted path to the goal is viable again, the intermediate attractor is replaced with the original goal pose. In the lower-left frame in Fig. 5, the attractive force is not active, as to not interfere with the Circular Fields force, facilitating local reactive obstacle evasion, and supplementing the global planning of MITA.

C. Comparative Analysis

We also performed quantitative experiments to evaluate the effectiveness of the proposed integrative approach and compare it against state-of-the-art reactive planners based on circular fields [26] with an additional safety margin to accommodate for the tool. Comparisons are made against the individual components of the planner, that is, ablation studies with respect to reactive tool rotation (RTR) and maneuverability-informed target assignment (MITA). To this end, we devised 30 different randomized scenarios instantiated with different environment conditions, e.g., initial $\boldsymbol{s}_{\text{start}}$ and goal $\boldsymbol{s}_{\text{goal}}$ configurations, as well as obstacle configurations. The scenarios were deployed for comparison between the four reactive planning strategies.

Table I summarizes the obtained results, which clearly depicts the advantages of the proposed planner. The RETOM planner only fails in two of the scenarios, one of them not being completed by any other analyzed approach as well. Furthermore, it is worth mentioning that the overall performance (along the successful trials) of 93% is also superior against baseline planners in terms of average path length and also average maneuverability score w_i of the traversed voxels along the path.

The baseline reactive planners have, in comparison, a poor success rate—which clearly highlights the relevance

TABLE I

COMPARISON BETWEEN THE PROPOSED APPROACH, ITS COMPONENTS, AND CIRCULAR FIELDS. QUANTITATIVE ASSESSMENT INCLUDES THE SUCCESS RATE, NUMBERS OF FAILURES DUE TO TOOL COLLISION (TOOL), END-EFFECTOR COLLISION (EE), JOINT-LIMITS (q_{LIM} AND SINGULARITIES ω. FOR PERFORMANCE ANALYSIS, AVERAGE PATH LENGTH (L) AND MANEUVERABILITY w. ARE COMPARED.

	Success	Failures			Performance	
	Rate	Tool/EE	q_{lim}	ω	$l(m)$	w
RETOM	**93%**	0/0	1	1	**0.93**	**0.073**
w/o MITA	60%	4/4	6	5	1.26	0.066
w/o RTR	83%	4/0	3	5	1.15	0.070
Circular Fields [26]	57%	5/3	5	5	1.24	0.067

of the proposed integrative approach from RETOM. Indeed, it is worth noticing the complementarity of MITA and RTR. Whilst MITA improves the path length and maneuverability, it is not able to address collisions with the tool (even with the additional safety margin). Furthermore, both exclusively local approaches (w/o MITA and Circular Fields) result in more convoluted longer paths, due to the lack of a global perspective, while average maneuverability is also lower among them. As expected, the advantages of tool reorientation are maximized in spaces with high maneuverability and the combined approach allows for improved performance and reactiveness. As MITA is updated at a lower frequency than the real-time reactive components, it can be computed separately and adds its benefit with negligible extra computation effort.

Limitations: While MITA aims to bridge global obstacle information with reactive planning strategies, it is crucial to acknowledge that it does not constitute a globally complete planner. This limitation is shared by all real-time planners. Instead, it employs heuristics informed by global obstacle and maneuverability information to bridge between global and local reactive features. There are no formal guarantees for finding a solution if one exists, or even ensuring the attractor and repulsive fields will keep the trajectory feasible within the workspace boundaries. Additionally, despite the advantages of CFs to avoid local minima, there are still limited conditions where it is formally guaranteed [44]. These limitations are notably influenced by parameter tuning, reflecting a common challenge faced by vector-field-based methodologies [45].

V. CONCLUSION AND FUTURE OUTLOOK

We proposed a reactive manipulation planner for tool maneuvers in semi-structured environments. Our capability-informed global planner captures the interaction between environmental wrenches for real-time evasive behaviors. We introduce the RETOM algorithm that generates Wrench-Fields while accounting for tool rotation in constrained spaces. The simulation studies conducted on a 7 DOF serial chain manipulator indicate that our novel framework is proficient in generating swift and obstacle-free paths in both static and dynamic scenarios. In the future, we plan to extend the approach to multi-agent exploration, including whole-body collision avoidance.

REFERENCES

[1] S. H. Johnson-Frey, "The neural bases of complex tool use in humans," *Trends in cognitive sciences*, vol. 8, no. 2, pp. 71–78, 2004.

[2] G. Federico, E. Reynaud, J. Navarro, M. Lesourd, V. Gaujoux, F. Lamberton, D. Ibarrola, C. Cavaliere, V. Alfano, M. Aiello *et al.*, "The cortical thickness of the area pf of the left inferior parietal cortex mediates technical-reasoning skills," *Scientific Reports*, vol. 12, no. 1, p. 11840, 2022.

[3] Y. Shirai, D. K. Jha, A. U. Raghunathan, and D. Hong, "Tactile tool manipulation," *arXiv preprint arXiv:2301.06698*, 2023.

[4] E. Sennesh, J. Theriault, D. Brooks, J.-W. van de Meent, L. F. Barrett, and K. S. Quigley, "Interoception as modeling, allostasis as control," *Biological Psychology*, vol. 167, p. 108242, 2022.

[5] M. Stilman and J. J. Kuffner, "Navigation among movable obstacles: Real-time reasoning in complex environments," *International Journal of Humanoid Robotics*, vol. 2, no. 04, pp. 479–503, 2005.

[6] M. Stilman, J.-U. Schamburek, J. Kuffner, and T. Asfour, "Manipulation planning among movable obstacles," in *Proceedings 2007 IEEE international conference on robotics and automation*. IEEE, 2007, pp. 3327–3332.

[7] H. Tian, C. Song, C. Wang, X. Zhang, and J. Pan, "Sampling-based planning for retrieving near-cylindrical objects in cluttered scenes using hierarchical graphs," *IEEE Transactions on Robotics*, 2022.

[8] K. Ellis, D. Hadjivelichkov, V. Modugno, D. Stoyanov, and D. Kanoulas, "Navigation among movable obstacles via multi-object pushing into storage zones," *IEEE Access*, 2023.

[9] C. R. Garrett, R. Chitnis, R. Holladay, B. Kim, T. Silver, L. P. Kaelbling, and T. Lozano-Pérez, "Integrated task and motion planning," *Annual review of control, robotics, and autonomous systems*, vol. 4, pp. 265–293, 2021.

[10] R. Holladay, T. Lozano-Pérez, and A. Rodriguez, "Force-and-Motion Constrained Planning for Tool Use," in *2019 IEEE/RSJ International Conference on Intelligent Robots and Systems (IROS)*, 2019.

[11] L. Chen, L. F. Figueredo, and M. R. Dogar, "Manipulation planning under changing external forces," *Autonomous Robots*, pp. 1–21, 2020.

[12] L. Chen, L. F. Figueredo, and M. Dogar, "Manipulation planning using environmental contacts to keep objects stable under external forces," in *2019 IEEE-RAS 19th International Conference on Humanoid Robots (Humanoids)*. IEEE, 2019, pp. 417–424.

[13] Z. Kingston, M. Moll, and L. E. Kavraki, "Sampling-based methods for motion planning with constraints," *Annual review of control, robotics, and autonomous systems*, vol. 1, pp. 159–185, 2018.

[14] R. Laha, R. Sun, W. Wu, D. Mahalingam, N. Chakraborty, L. F. Figueredo, and S. Haddadin, "Coordinate invariant user-guided constrained path planning with reactive rapidly expanding plane-oriented escaping trees," in *2022 International Conference on Robotics and Automation (ICRA)*. IEEE, 2022, pp. 977–984.

[15] C.-A. Cheng, M. Mukadam, J. Issac, S. Birchfield, D. Fox, B. Boots, and N. Ratliff, "Rmpflow: A geometric framework for generation of multitask motion policies," *IEEE Transactions on Automation Science and Engineering*, vol. 18, no. 3, pp. 968–987, 2021.

[16] A. Bylard, R. Bonalli, and M. Pavone, "Composable geometric motion policies using multi-task pullback bundle dynamical systems," in *2021 IEEE International Conference on Robotics and Automation (ICRA)*. IEEE, 2021, pp. 7464–7470.

[17] K. Van Wyk, M. Xie, A. Li, M. A. Rana, B. Babich, B. Peele, Q. Wan, I. Akinola, B. Sundaralingam, D. Fox *et al.*, "Geometric fabrics: Generalizing classical mechanics to capture the physics of behavior," *IEEE Robotics and Automation Letters*, vol. 7, no. 2, pp. 3202–3209, 2022.

[18] O. Khatib, "Real-time obstacle avoidance for manipulators and mobile robots," in *Proceedings. 1985 IEEE International Conference on Robotics and Automation*. Institute of Electrical and Electronics Engineers, 1985, pp. 500–505.

[19] J.-O. Kim and P. Khosla, "Real-time obstacle avoidance using harmonic potential functions," *IEEE Transactions on Robotics and Automation*, 1992.

[20] L. Singh, H. Stephanou, and J. Wen, "Real-time robot motion control with circulatory fields," in *Proceedings of IEEE International Conference on Robotics and Automation*, vol. 3. IEEE, 1996, pp. 2737–2742.

[21] L. Singh, J. Wen, and H. Stephanou, "Motion planning and dynamic control of a linked manipulator using modified magnetic fields," in *Proceedings of International Conference on Robotics and Automation*, vol. 2. IEEE, 1997, pp. 1142–1147.

[22] E. Rimon and D. E. Koditschek, "Exact robot navigation using artificial potential functions," *Departmental Papers (ESE)*, p. 323, 1992.

[23] G. Garimella, M. Sheckells, and M. Kobilarov, "A stabilizing gyroscopic obstacle avoidance controller for underactuated systems," in *2016 IEEE 55th Conference on Decision and Control (CDC)*. IEEE, 2016, pp. 5010–5016.

[24] S. Haddadin, R. Belder, and A. Albu-Schäffer, "Dynamic motion planning for robots in partially unknown environments," *IFAC Proceedings Volumes*, vol. 44, no. 1, pp. 6842–6850, jan 2011.

[25] A. Ataka, H.-K. Lam, and K. Althoefer, "Reactive magnetic-field-inspired navigation method for robots in unknown convex 3-d environments," *IEEE Robotics and Automation Letters*, vol. 3, no. 4, pp. 3583–3590, 2018.

[26] R. Laha, L. F. Figueredo, J. Vrabel, A. Swikir, and S. Haddadin, "Reactive cooperative manipulation based on set primitives and circular fields," in *2021 IEEE International Conference on Robotics and Automation (ICRA)*. IEEE, may 2021, pp. 6577–6584.

[27] K. M. Lynch and F. C. Park, *Modern Robotics*. Cambridge University Press, 2017.

[28] A. Billard, S. Mirrazavi, and N. Figueroa, *Learning for Adaptive and Reactive Robot Control: A Dynamical Systems Approach*. MIT Press, 2022.

[29] L. Huber, J.-J. Slotine, and A. Billard, "Avoidance of concave obstacles through rotation of nonlinear dynamics," *IEEE Transactions on Robotics*, 2023.

[30] M. Becker, T. Lilge, M. A. Müller, and S. Haddadin, "Circular fields and predictive multi-agents for online global trajectory planning," *IEEE Robotics and Automation Letters*, vol. 6, no. 2, pp. 2618–2625, 2021.

[31] R. Laha, J. Vorndamme, L. F. Figueredo, Z. Qu, A. Swikir, C. Jähne, and S. Haddadin, "Coordinated motion generation and object placement: A reactive planning and landing approach," in *2021 IEEE/RSJ International Conference on Intelligent Robots and Systems (IROS)*. IEEE, 2021, pp. 9401–9407.

[32] R. Laha, M. Becker, J. Vorndamme, J. Vrabel, L. F. Figueredo, M. A. Müller, and S. Haddadin, "Predictive multi-agent based planning and landing controller for reactive dual-arm manipulation," *IEEE Transactions on Robotics*, 2023.

[33] K. C. Gupta and B. Roth, "Design Considerations for Manipulator Workspace," *Journal of Mechanical Design*, vol. 104, no. 4, 10 1982.

[34] Z. Wang, S. Ji, Y. Li, and Y. Wan, "A unified algorithm to determine the reachable and dexterous workspace of parallel manipulators," *Robotics and Computer-Integrated Manufacturing*, vol. 26, no. 5, 2010.

[35] S. Patel and T. Sobh, "Manipulator Performance Measures - A Comprehensive Literature Survey," *Journal of Intelligent and Robotic Systems: Theory and Applications*, vol. 77, no. 3-4, pp. 547–570, 2014.

[36] Y. Han, J. Pan, M. Xia, L. Zeng, and Y.-J. Liu, "Efficient se (3) reachability map generation via interplanar integration of intra-planar convolutions," in *IEEE Int. Conf. Robotics & Automation (ICRA)*, 2021.

[37] H. Yao, R. Laha, L. F. Figueredo, and S. Haddadin, "Enhanced dexterity maps (edm): A new map for manipulator capability analysis," *IEEE Robotics and Automation Letters*, 2023.

[38] M. Becker, P. Caspers, T. Hattendorf, T. Lilge, S. Haddadin, and M. A. Müller, "Informed circular fields for global reactive obstacle avoidance of robotic manipulators," *arXiv preprint arXiv:2212.05815*, 2022.

[39] T. Yoshikawa, "Manipulability of robotic mechanisms," *The international journal of Robotics Research*, vol. 4, no. 2, pp. 3–9, 1985.

[40] Y. Koren and J. Borenstein, "Potential field methods and their inherent limitations for mobile robot navigation," in *Proceedings. 1991 IEEE International Conference on Robotics and Automation*. IEEE Comput. Soc. Press, 1991, pp. 1398–1404.

[41] S. Patel and T. Sobh, "Manipulator performance measures-a comprehensive literature survey," *Journal of Intelligent & Robotic Systems*, vol. 77, pp. 547–570, 2015.

[42] E. Rohmer, S. P. Singh, and M. Freese, "V-rep: A versatile and scalable robot simulation framework," in *2013 IEEE/RSJ International Conference on Intelligent Robots and Systems*. IEEE, 2013.

[43] B. V. Adorno and M. M. Marinho, "Dq robotics: A library for robot modeling and control," *IEEE Robotics Automation Magazine*, 2020.

[44] M. Becker, J. Köhler, S. Haddadin, and M. Müller, "Motion planning using reactive circular fields: A 2-d analysis of collision avoidance and goal convergence," *IEEE Transactions on Automatic Control*, vol. PP, pp. 1–16, 01 2023.

[45] A. Sinha, R. Laha, and N. Chakraborty, "Oc3: A reactive velocity level motion planner with complementarity constraint-based obstacle avoidance for mobile robots," in *2023 IEEE 19th International Conference on Automation Science and Engineering (CASE)*. IEEE, 2023, pp. 1–8.